Fabrication of a Targeted Drug Delivery System from a Pillar[5]arene-Based Supramolecular Diblock Copolymeric Amphiphile for Effective Cancer Therapy

*Guocan Yu, Wei Yu, Li Shao, Zhihua Zhang, Xiaodong Chi, Zhengwei Mao, Changyou Gao, and Feihe Huang**

Effective cancer therapy will profit from the development of sophisticated drug delivery systems with stimuli-responsive properties that are capable of delivering therapeutic doses to the active sites, while minimizing the accumulation of highly toxic drugs in off-target sites. Herein, the fabrication of a pillararene-based amphiphilic supramolecular diblock polymer (P5-PEG-Biotin⊃PCL-C_2V) based on the host–guest recognition between a water-soluble pillar[5]arene and a viologen salt is reported. P5-PEG-Biotin⊃PCL-C_2V self-assembles into polymersomes, which are utilized as drug delivery vehicles for doxorubicin hydrochloride (DOX). Decorated by the biotin groups, these smart nanocarriers deliver the anticancer drug preferentially to biotin receptor over-expressing cancer cells. After internalization by the cells, the viologen group is reduced into the cationic radical state by the intracellular reductase NAD(P)H, leading to the release of the loaded DOX by the disassembly of the polymersomes. More importantly, DOX-loaded polymersomes maintain the therapeutic efficacy towards cancerous HeLa cells, while exhibiting relatively low cytotoxicity towards normal HEK293 cells. In vivo studies reveal that the DOX-loaded supramolecular polymersomes prolong the circulation time in the bloodstream, promote the antitumor efficacy and reduce the systematic toxicity of the drug through flexible and modular supramolecular strategy.

1. Introduction

Over the past decades, stimuli-responsive drug delivery systems (DDSs) with targeting ability have received extensive attention in cancer therapy due to their enhanced pharmacokinetics and pharmacodynamics.[1] The use of smart DDSs can overcome several problems that are associated with traditional drugs, such as low bioavailability, poor aqueous solubility and nonspecific distribution in the body.[2] It is an important and growing area of research to develop DDSs that respond to the intrinsic stimuli characteristic of the pathological site, greatly reducing side effect to the normal tissues.[3] In order to realize these functions, the core issue is to exploit sophisticated delivery vehicles. Among various drug delivery vehicles, polymersomes with an aqueous interior enclosed by a hydrophobic bilayer membrane have been increasingly used as powerful tools for drug delivery.[4] However, for the most reported polymer blocks of amphiphilic block copolymers whose monomers were connected by covalent bonds, intricate polymer and/or organic synthesis was required to tune the functional properties of the polymersomes by engineering the blocks of the starting copolymers. On the other hand, it is not easy to realize controlled disassembly due to covalent connections between the blocks in block copolymers that are short of stimuli-responsiveness.

Recently, a series of supramolecular block copolymers were fabricated through a "block-copolymer-free" strategy by orthogonal assembly of two or three homopolymers through noncovalent interactions at chain ends, such as hydrogen bonding, metal-ligand coordination, and host–guest interactions.[5] Polymersomes fabricated from supramolecular block copolymers based on host–guest interactions especially exhibited more and more advantages as DDSs in cancer therapy, because the structures of DDSs can be controlled based on the high self-selectivity of host–guest interactions and the drug release can be triggered by various stimuli at active sites based on the rich environment-responsiveness of host–guest interactions.[6] Pillararenes[7] are a new class of macrocyclic hosts next to calixarenes, cyclodextrins, crown ethers and cucurbiturils. The unique symmetrical architecture and easy functionalization of pillar[*n*]arenes have afforded them excellent properties in the construction of interesting host–guest chemistry and provided a useful platform for the fabrication of various stimuli-responsive supramolecular systems.[8] A series of stimuli-responsive supra-amphiphiles constructed from pillararene-based host–guest recognition have been reported.[9] However, most of these

G. Yu, L. Shao, Z. Zhang, X. Chi, Prof. F. Huang
State Key Laboratory of Chemical Engineering
Center for Chemistry of
High-Performance & Novel Materials
Department of Chemistry
Zhejiang University
Hangzhou 310027, P. R. China
E-mail: fhuang@zju.edu.cn
W. Yu, Prof. Z. Mao, Prof. C. Gao
MOE Key Laboratory of Macromolecular Synthesis and Functionalization
Department of Polymer Science and Engineering
Zhejiang University
Hangzhou 310027, P. R. China

DOI: 10.1002/adfm.201601770

studies focused on small molecular supra-amphiphiles, limiting their applications in drug delivery due to their low thermodynamic stability and durability. On account of their fascinating host–guest properties, it is extremely timely to fabricate stimuli-responsive polymersomes self-assembled from pillar[*n*]arene-based supramolecular block copolymers as targeting DDSs.

Herein, we combined the concept of "block-copolymer-free" strategy with pillararene-based host–guest chemistry, and successfully prepared a pillararene-based amphiphilic supramolecular diblock copolymer and used it in targeted drug delivery. Poly(ethylene glycol) (PEG) functionalized with a triglycol monomethyl ether-modified pillar[5]arene host unit and a biotin targeting group (**P5-PEG-Biotin**) and poly(caprolactone) bearing a viologen terminator (**PCL-C_2V**) were designed as hydrophilic and hydrophobic segments, respectively (**Figure 1**). As shown in Figure 1, these two segments were linked by pillararene-based host–guest recognition to form an amphiphilic supramolecular diblock copolymer **P5-PEG-Biotin⊃PCL-C_2V**, which self-assembled into polymersomes in water. These polymersomes were employed as drug delivery vehicles to encapsulate anticancer drug doxorubicin hydrochloride (DOX). The biotin ligands decorating the surfaces of the vesicles endowed these vehicles with excellent targeting ability to deliver DOX preferentially to biotin receptor-positive HeLa cancer cells. After internalization by the cells, the host–guest interactions were destroyed by the reduction of the viologen group into its cationic radical state by the intracellular reductase NAD(P)H, resulting in the release of the loaded DOX concomitantly with disassembly of the vesicles. The therapeutic efficacy of DOX was retained for cancer cells, while its cytotoxicity towards normal cells was greaty reduced. The potency of this sophisticated supramolecular drug delivery system in cancer therapy was evaluated in HeLa tumor-bearing mice. In vivo experiments revealed that the DOX-loaded supramolecular polymersomes prolonged the circulation time in bloodstream, promoted the antitumor efficacy and reduced the systematic toxicity of the drug through flexible and modular supramolecular strategy.

2. Results and Discussion

2.1. Investigations of the Host–Guest Molecular Recognition

C_5V (Figure 1) was utilized as a model compound to investigate the host–guest complexation between model host **P5** (Figure 1) and viologen group on **PCL-C_2V** through ^{1}H NMR

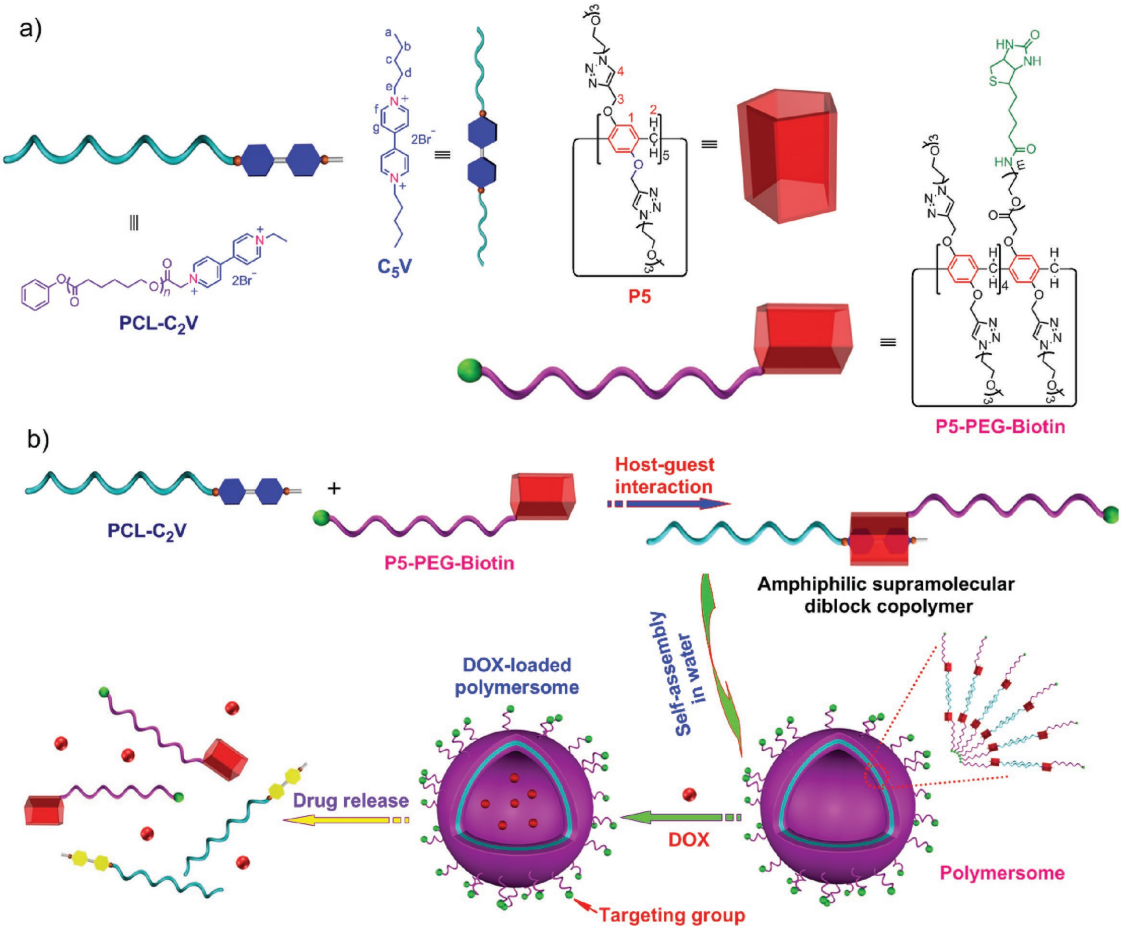

Figure 1. a) Chemical structures and cartoon representations of **C_5V**, **P5**, **P5-PEG-Biotin** and **PCL-C_2V**. b) Schematic illustration of the formation of polymersomes self-assembled from the amphiphilic supramolecular copolymer **P5-PEG-Biotin⊃PCL-C_2V** and their use as reduction-responsive drug delivery vehicles.

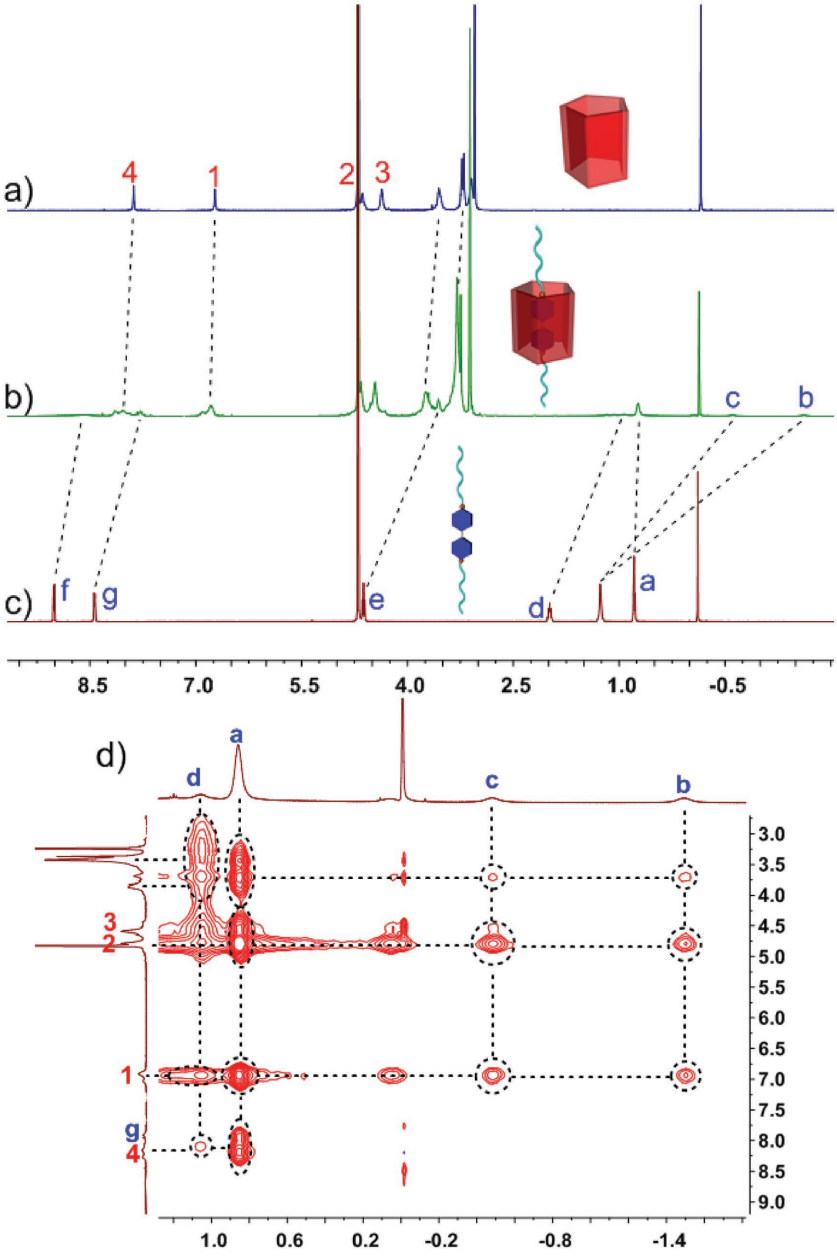

Figure 2. Partial ^{1}H NMR spectra (400 MHz, D_2O, 295 K): a) **P5** (1.00 mM); b) **P5** (1.00 mM) and $\mathbf{C_5V}$ (1.00 mM); c) $\mathbf{C_5V}$ (1.00 mM). d) 2D NOESY NMR spectrum (500 MHz, D_2O, 295 K) of **P5** (10.0 mM) and $\mathbf{C_5V}$ (10.0 mM). The graph axes present the chemical shifts and the units are ppm.

spectroscopy (**Figure 2**). In comparison with free $\mathbf{C_5V}$, the resonance signals of the protons on $\mathbf{C_5V}$ exhibited upfield shifts upon addition of 1.0 equivalent of **P5** (Figure 2, spectra (b c). Especially, the signals of protons H^b and H^c were found below zero, because these protons were located in the cavity of **P5** and shielded by the electron-rich cyclic structure upon formation of an inclusion complex between **P5** and $\mathbf{C_5V}$.[8a] On the other hand, a broadening effect was observed for the peaks corresponding to protons H^b, H^c, H^d and H^f due to the complexation dynamics.[9a] The signals corresponding to the protons on **P5** also exhibited slight chemical shift changes caused by the host–guest interaction between **P5** and $\mathbf{C_5V}$. In order to study the relative positions of the building blocks in the host–guest inclusion complex, 2D NOESY NMR spectroscopy was conducted. Strong NOE correlations were observed between the resonance peaks of the protons on $\mathbf{C_5V}$ and the protons of **P5**, suggesting that $\mathbf{C_5V}$ was deeply threaded into the cavity of **P5**, which was in good agreement with the results obtained from ^{1}H NMR investigations.

UV–Vis absorption spectroscopy provided further evidence for the complexation between **P5** and $\mathbf{C_5V}$. When **P5** and $\mathbf{C_5V}$ were mixed in 1:1 molar ratio, the obtained solution had a yellow color (Figure S23), confirming the formation of a charge-transfer (CT) complex. The UV–vis spectrum of this solution exhibited a broad absorption above 400 nm (Figure S23), corresponding to the typical absorption of the pillar[5]arene/paraquat CT complex.[10] Fluorescence titration experiments were conducted to determine the association constant (K_a) for the complexation between **P5** and $\mathbf{C_5V}$ (Figure S17). Upon gradual addition of $\mathbf{C_5V}$ into the solution containing **P5**, the fluorescence intensity at 330 nm was quenched obviously, arising from the effective host–guest complexation. The stoichiometry of this host–guest complex was determined to be 1:1 by a mole ratio based on the fluorescence titration experiments (Figure S18). Additionally, the K_a value was measured to be $(1.14 \pm 0.11) \times 10^4$ M^{-1} by using a non-linear curve-fitting method (Figure S19). The driving forces for the formation of $\mathbf{P5}\supset\mathbf{C_5V}$ were attributed to the cooperativity of hydrophobic and charge transfer interactions between electron-poor $\mathbf{C_5V}$ and electron-rich **P5**. A low-resolution electrospray ionization mass spectroscopy peak at m/z 1589.9 (Figure S24) was monitored, corresponding to $[\mathbf{P5}\supset\mathbf{C_5V} - 2Br]^{2+}$, further confirming the formation of 1:1 host–guest complex between **P5** and $\mathbf{C_5V}$.

2.2. Fabrication of Reduction-Triggered Supramolecular Polymersomes

After the establishment of the new and efficient host–guest recognition motif based on **P5** and $\mathbf{C_5V}$, it was used to fabricate an amphiphilic supramolecular diblock copolymer (**P5-PEG-Biotin⊃PCL-$\mathbf{C_2V}$**) with the PEG segment as the hydrophilic part and the PCL segment as the hydrophobic section. The critical aggregation concentration (CAC) of **P5-PEG-Biotin⊃PCL-$\mathbf{C_2V}$** was estimated to be 0.23 mg mL^{-1} by the fluorescent probe method using pyrene as a probe molecule (Figure S25).

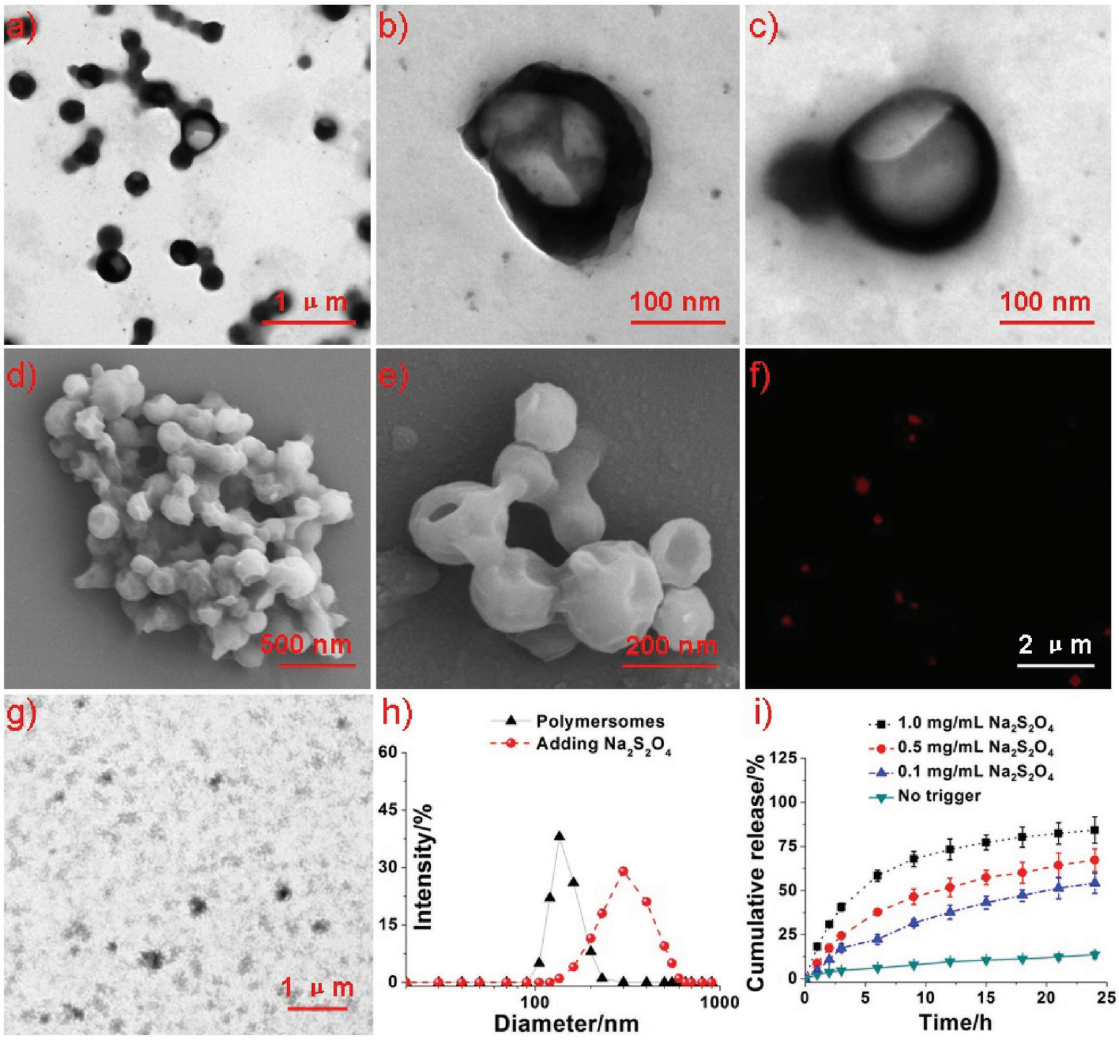

Figure 3. a–c) TEM images of the polymersomes self-assembled from **P5-PEG-Biotin⊃PCL-C_2V**. d,e) SEM images of the polymersomes self-assembled from **P5-PEG-Biotin⊃PCL-C_2V**. f) Confocal laser scanning microscopy (CLSM) image of the DOX-loaded polymersomes. g) TEM image of the polymersomes in the presence of $Na_2S_2O_4$ (0.1 mg mL^{-1}). h) DLS size distributions of the polymersomes in the absence and presence of $Na_2S_2O_4$ (0.1 mg mL^{-1}). i) Release profiles of DOX-loaded polymersomes with or without different concentrations of $Na_2S_2O_4$.

Transmission electron microscopy (TEM) and dynamic light scattering (DLS) studies were conducted to determine the morphology and size of these nanoaggregates (**Figure 3**). As shown in Figure 3a, spherical aggregates with diameter of ~150 nm were clearly observed in the TEM image. As evidenced by the distinct contrast between the hollow part and periphery (Figure 3c), we knew that these self-assemblies were polymersomes. From the enlarged TEM image (Figure 3b), we found that the membrane of the polymersomes collapsed and wrinkled in the drying process. The wall thickness was estimated to be about 15 nm by TEM statistics, in agreement with the bilayer molecular length of **P5-PEG-Biotin⊃PCL-C_2V**,[5a] indicating orthogonal assembly fashion in aqueous solution. The size was close to the result obtained from the DLS measurement, which gave an average size of 137 nm (Figure 3h). SEM images provided further convincing evidence for the formation of polymersomes self-assembled from **P5-PEG-Biotin⊃PCL-C_2V**. As shown in Figure 3d and 3e, some wrinkled vesicles and ruptured polymersomes were clearly observed.

The inner cavities of these polymersomes were hydrophilic and thus could be utilized to encapsulate water soluble cargoes. Therefore, the formation of vesicles was also confirmed by confocal laser scanning microscopy (CLSM) by encapsulating red-emitting doxorubicin hydrochloride (DOX) in the aqueous interior (Figure 3f). To prepare DOX-loaded polymersomes, **P5-PEG-Biotin⊃PCL-C_2V** in THF was injected dropwise into an aqueous solution of DOX under stirring, and after standing overnight, unloaded DOX was removed by dialysis against water. As a result, DOX was successfully loaded into the polymersomes formed from **P5-PEG-Biotin⊃PCL-C_2V**. The drug loading efficiency was estimated to be 16.7%. Compared with the free polymersomes, the absorption of DOX-loaded vesicular solution from 500 to 660 nm becomes much stronger (Figure S28), which reflects the characteristic absorption of DOX. Moreover, the DOX-loaded vesicular solution turns dark

red, different from the light brown unloaded vesicular solution, demonstrating that DOX was successfully encapsulated into the polymersomes (Figure S28).

Viologens can be reduced into the corresponding cationic radical state by the intracellular reductase, such as NAD(P)H.[11] As a consequence, the pillar[5]arene/viologen host–guest interactions were reduced significantly, resulting in the disassembly of the polymersomes. From fluorescence titration experiments, the K_a value of **P5⊃C$_2$V$^{+\cdot}$** was calculated to be $(1.61 \pm 0.13) \times 10^2$ M^{-1} (Figure S22), 70 times lower than the corresponding value of **P5⊃C$_5$V**. In order to mimic the intracellular reduction environment, a reducing agent sodium dithionite ($Na_2S_2O_4$) was utilized to investigate the reduction-triggered disassembly of the polymersomes. As shown in the TEM image (Figure 3g), the vesicles were disrupted, resulting in the formation of irregular aggregates in the presence of $Na_2S_2O_4$ (0.1 mg mL^{-1}). The solution transformed from transparent to turbid in this process due to the precipitation of **PCL-C$_2$V$^{+\cdot}$** from the aqueous solution which confirmed that the pillar[5]arene/viologen binding was significantly weakened by the reducing agent. The reduction-triggered disassembly process was also monitored by DLS measurements (Figure 3h). The mean diameter of the nanoaggregates changed from 137 nm to 350 nm by culturing the polymersomes with an aqueous solution containing $Na_2S_2O_4$ for 12 h, in line with the result obtained from TEM studies. Accompanied with the collapse of the polymersomes, the encapsulated DOX within their interior was released, suggesting that these polymersomes could serve as drug delivery vehicles. Drug release profiles of DOX-loaded supramolecular polymersomes in the absence or presence of different amounts of $Na_2S_2O_4$ are compared in Figure 3i. The loaded DOX was released faster from the polymersomes after adding higher concentrations of $Na_2S_2O_4$. In the absence of $Na_2S_2O_4$, only 13.6% DOX was released within 24 h, whereas 54.2%, 67.3% and 84.3% DOX were released in the same time scale in the presence of 0.1, 0.5 and 1.0 mg/mL $Na_2S_2O_4$, respectively, which confirmed reduction-triggered disassembly of the polymersomes. The covalent-linked diblock polymer **Biotin-PEG-*b*-PCL** was utilized as a control, which self-assembled into nanoparticles in aqueous solution with the diameter about 100 nm. The hydrophobic core of the nanoparticles was used to encapsulate neutral DOX through hydrophobic interactions. The release behaviors showed that negligible changes were monitored in the absence and presence of $Na_2S_2O_4$ (Figure S27), confirming the reduction-triggered release arose from the disassociation of the host–guest interactions.

2.3. In vitro Targeted Drug Delivery Studies

A major concern in cancer chemotherapy is the low therapeutic efficacy of the drugs utilized, which can be partially improved by employing anticancer drugs that are specifically targeted to cancer cells. Until now, various targeting species have been utilized to modify the nanocarrier vehicles, such as lectins, sugars, vitamins, and peptides.[12] Rapidly dividing cancerous cells have a voracious appetite for certain vitamins, such as biotin (vitamin B_7), vitamin B_{12} and folate (vitamin B_9).[12b] It has been found that the biotin level is much higher in some cancerous cells compared with normal cells. Some tumor cell lines including colorectal, ovarian etc., which over-express receptors involved in vitamin B_9 or vitamin B_{12} uptake also exhibited over-expression of biotin receptors. In this study, the DOX-loaded polymersomes were decorated by biotin on the surfaces, thus possessing the ability to specifically deliver DOX to biotin receptor over-expressing cancer cells, minimizing systemic distribution of the drug.

In order to work as targeting and efficient universal scaffolds for drug delivery, the nanocarriers should be biocompatible. Compared with some synthetic polymers with complex structures, both PCL and PEG are FDA-approved polymers with excellent biocompatibility and wide availability, making them ideal candidates for bio-relevant applications. Considering the potential applications of these polymersomes in the field of drug delivery, their cytotoxicity was evaluated by a 3-(4′,5′-dimethylthiazol-2′-yl)-2,5-diphenyl tetrazolium bromide (MTT) assay. Negligible changes were monitored in relative cell viability in the presence of **P5-PEG-Biotin⊃PCL-C$_2$V** with the concentrations ranging from 50 to 250 μg mL^{-1} (Figure S30), indicating low cytotoxicity and excellent biocompatibility of these polymersomes.

After internalization by the cells, the viologen group was reduced into its cationic radical state by NAD(P)H, resulting in the release of the loaded DOX due to the disassembly of the polymersomes. CLSM and flow cytometry (FCM) investigations were conducted to verify whether the biotin moieties decorating the surfaces of the polymersomes could guide these nanocarriers preferentially to biotin receptor overexpressed cancer cells (HeLa cells), rather than normal cells (HEK293 cells) with lower density of biotin receptors. Upon incubation with DOX-loaded polymersomes (the concentration of DOX was 5.00 μM) for 2 h, red fluorescence was observed mainly in the cytoplasm of HeLa cells, indicating that the encapsulated DOX was released (**Figure 4**a). By extending the culture time to 4 h, the fluorescence of DOX was mostly localized in the nucleus and the corresponding fluorescence intensity increased significantly. In contrast, HEK293 cells showed a weak fluorescence signal under the same experimental condition (Figure 4a), confirming that the self-assembled polymersomes from **P5-PEG-Biotin⊃PCL-C$_2$V** with biotin groups contributed to the enhanced cancer cell-specific uptake.

The level of DOX-loaded polymersomes internalized in HeLa and HEK293 cells was quantified by FCM. Figure 4b and 4c show that HeLa cells have a faster uptake rate and higher intracellular accumulation of DOX-loaded polymersomes than HEK293 cells. As shown by FCM, the HeLa cells ingested 4.7 times of the biotinylated polymersomes than the HEK293 cells (mean fluorescent intensity of 39.2 vs 8.31) after incubation with the DOX-loaded polymersomes for 2 h (Figure 4b and c). The cellular uptake of biotinylated DOX-loaded polymersomes was also measured after pretreatment of cells with free biotin (100 μM, 0.5 h) to block the biotin receptors, further providing evidence for the targeting ability of the polymersomes. For HeLa cells cultured with the DOX-loaded polymersomes for 2 h, the pretreatment with biotin for 0.5 h caused the significant inhibition of cellular uptake of the polymersomes, evidenced with the fluorescent intensity per cell reduced from 39.2 to 11.7. For HEK293 cells, pre-treatment with free biotin

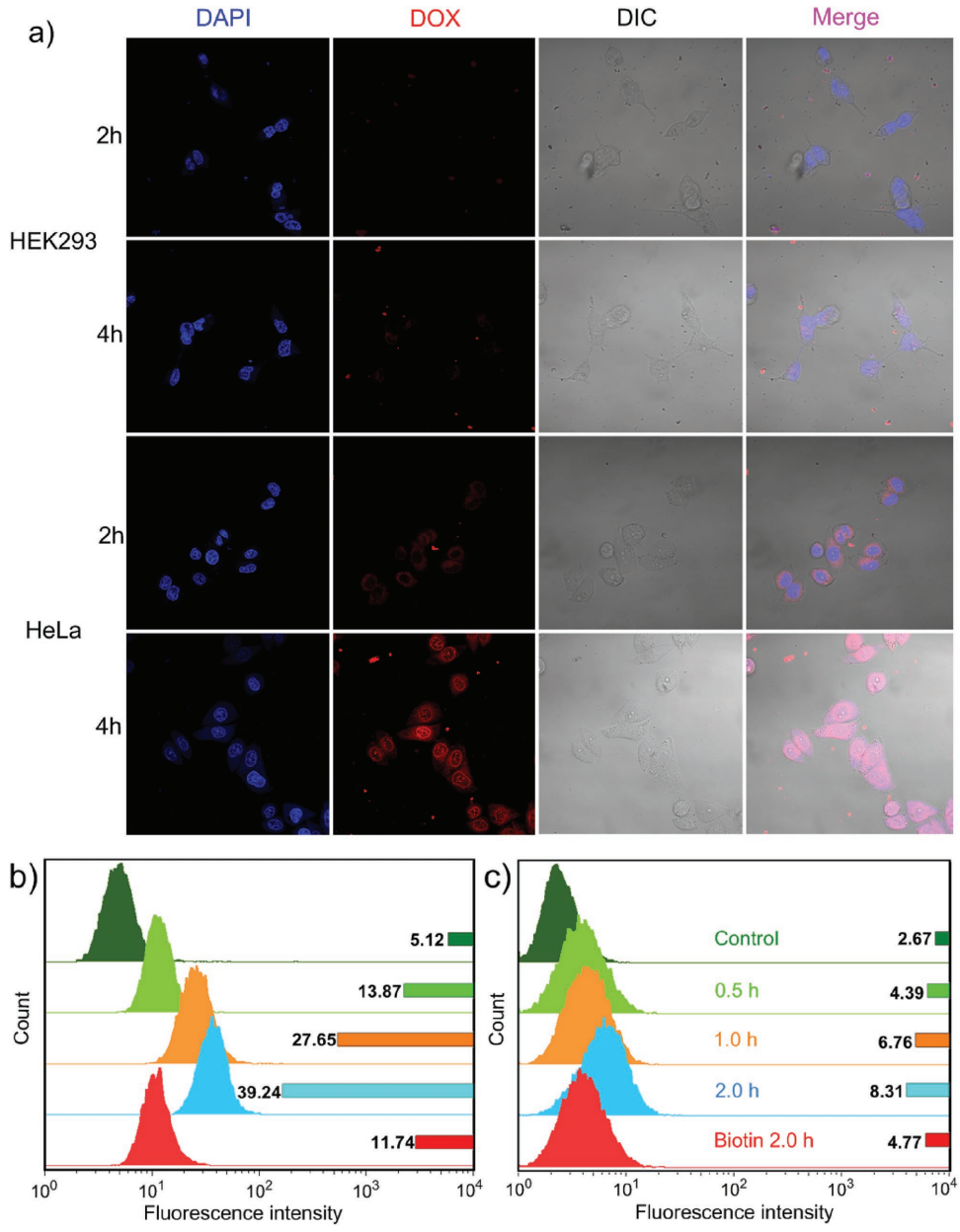

Figure 4. a) CLSM images of the HeLa and HEK293 cells incubated with the DOX-loaded polymersomes. Flow cytometry analysis results of fluorescence signals collected in b) HeLa and c) HEK-293 cells after treatment with the DOX-loaded polymersomes for different times in the absence and presence of biotin. Cells without any treatment were regarded as the control groups. The concentration of DOX was 5.00 μM.

had negligible effect on the cellular uptake of the polymersomes, confirming ligand–receptor interaction nature between the biotin modified polymersomes and the HeLa cells. These phenomena demonstrated that the introduction of biotin significantly improved the specific targeting ability of the polymersomes towards biotin receptor-overexpressing cancer cells via receptor-mediated endocytosis.

To further confirm targeted drug delivery by these supramolecular polymersomes and evaluate the anticancer efficiency of DOX-loaded polymersomes, MTT assay were performed. Free DOX or DOX-loaded polymersomes were cultured with HeLa (**Figure 5**b) and HEK293 (Figure 5a) cells with or without pretreatment of biotin, respectively. The relative cell viability in different groups was recorded after 24 h incubation. As shown in Figure 5b, the relative cell viability cultured with the free DOX and DOX-loaded polymersomes decreases gradually with increasing concentration of DOX from 5 μg mL^{-1} to 25 μg mL^{-1}, demonstrating that the efficacy of the anticancer drug was maintained effectively. From comparison of these two groups (Figure 5b), we can know that the relative cell viability of the cells cultured with free DOX is a little lower than that of the DOX-loaded polymersomes, because the cationic DOX can diffuse into the cells easily. In comparison with the HeLa cells, the DOX-loaded polymersomes exhibited reduced dose-dependent

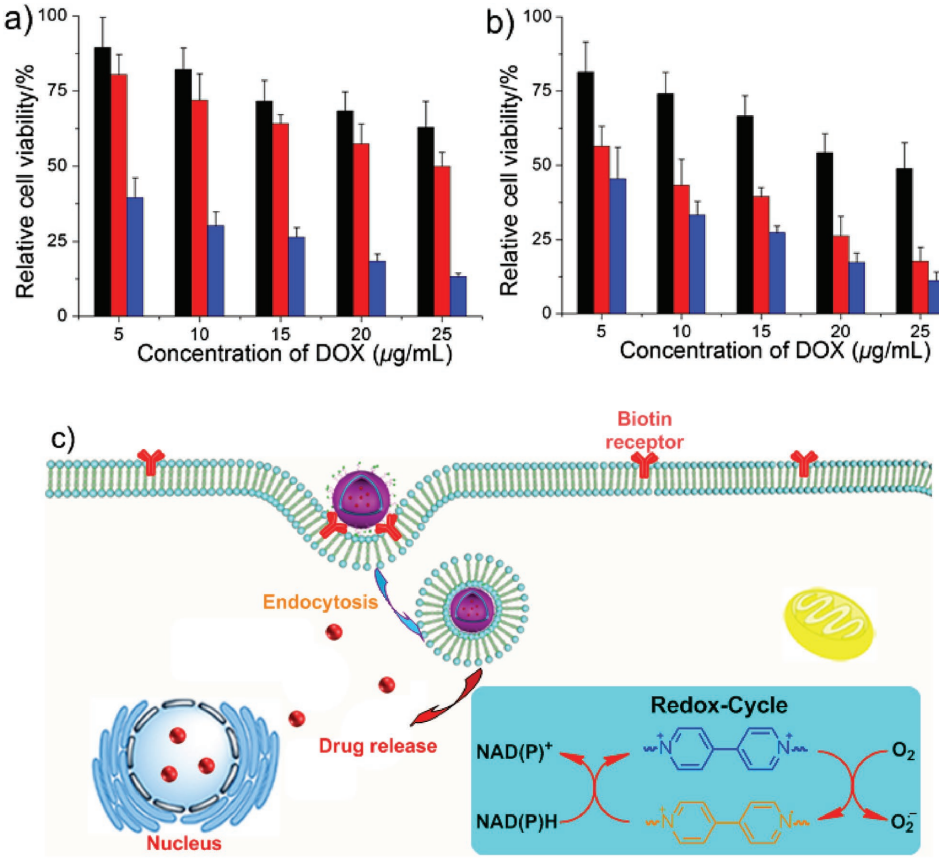

Figure 5. Cytotoxicity of a) HEK293 and b) HeLa cells with different treatments: DOX-loaded polymersomes (black column); free DOX (blue column); pretreated with free biotin and then with DOX-loaded polymersomes (red column). The concentration of DOX was tuned by changing the amount of the added DOX in the preparation of DOX-loaded polymersomes. The concentration of the supramolecular diblock polymer was kept at 0.25 mg mL^{-1}, which was higher than the corresponding CAC. c) Schematic illustration of the targeted drug delivery and the reduction-triggered drug release.

antiproliferative activity against HEK293 cells with low biotin receptor levels (Figure 5a); this demonstrated that DOX-loaded polymersomes specifically delivered the anticancer drug to the cancer cells rather than the normal cells. More importantly, the cytotoxicity of the DOX-loaded polymersomes towards HeLa cells decreased significantly by treatment with free biotin (100 μM, 0.5 h) prior to incubating with the polymersomes to block the receptors (Figure 5b). However, the decrease in cytotoxicity against HEK293 cells was much lower by pretreatment with biotin (Figure 5a), providing further evidence for the receptor-mediated uptake. It should be emphasized that the cytotoxicity of the DOX-loaded nanoparticles fabricated from **Biotin-PEG-*b*-PCL** was lower than that of the DOX-loaded polymersomes towards both HeLa and HEK293 cells at the same concentration. The reason was that **Biotin-PEG-*b*-PCL** linked by a covalent bond was short of stimuli-responsiveness, thus the loaded neutral DOX could be hardly released from the obtained nanoparticles. In conjunction with the results obtained from CLSM, FCM and MTT assay, we conclude that the polymersomes self-assembled from the amphiphilic supramolecular diblock copolymer preferentially delivered the anticancer drug to the biotin receptor over-expressing cancer cells via receptor-mediated endocytosis to kill the cancer cells selectively, with reduced side effects to normal tissues.

2.4. In vivo Tumor Inhibition

Compared with free small molecule weight drugs, nancarriers with a suitable size always possess a longer retention time in the blood stream via the enhanced permeability and retention (EPR) effect.[13] On the other hand, the PEG segments of the polymersomes prevent themselves from being recognized by body's biological particulate filters, further prolonging their circulation time in blood.[14] The in vitro stability of the DOX-loaded polymersomes was evaluated in PBS buffer supplemented with 10% fetal bovine serum at 37 °C. No obvious size variation of the DOX-loaded polymersomes was observed over 20 h, confirming the excellent colloidal and chemical stability (Figure S29). Rather than the difference in the reduction-responsive ability, there existed a lot of influencing factors on the in vivo results treated with the DOX-loaded nanoparticles or the DOX-loaded polymersomes, such as the stabilities in delivery process, endocytic pathways, released behaviors, excretions and so on. Therefore, we only investigated the anticancer efficacy of the DOX-loaded polymersomes in vivo to demonstrate that this novel biocompatible supramolecular material could be potentially used in cancer treatment. The pharmacokinetics of free DOX and DOX-loaded polymersomes following intravenous (i.v.) injection in mice was investigated and the

plasma concentration of DOX was determined by high performance liquid chromatography (HPLC) at various time points. As shown in the concentration-time curve after administration of free DOX and DOX-loaded polymersomes (**Figure 6**a), the blood retention time of DOX-loaded polymersomes was longer than that of free DOX and the corresponding area under the curve was larger, demonstrating that the circulation time of the DOX-loaded polymersomes was enhanced significantly, which provided the possibility of enhanced drug accumulation in the tumor. The effective tumor targeting of DOX-loaded polymersomes was verified by quantification analysis of DOX amounts in tumor tissue and other main organs after 12 h post-injection. DOX administrated alone exhibited very low accumulation in tumor, while relatively high accumulation in lung, liver and kidney, indicating that the free DOX could not improve the tumor uptake of DOX. In contrast to the free DOX, the concentration of DOX was remarkably higher in the tumor (about 3-fold) and lower in the main organs after treatment with

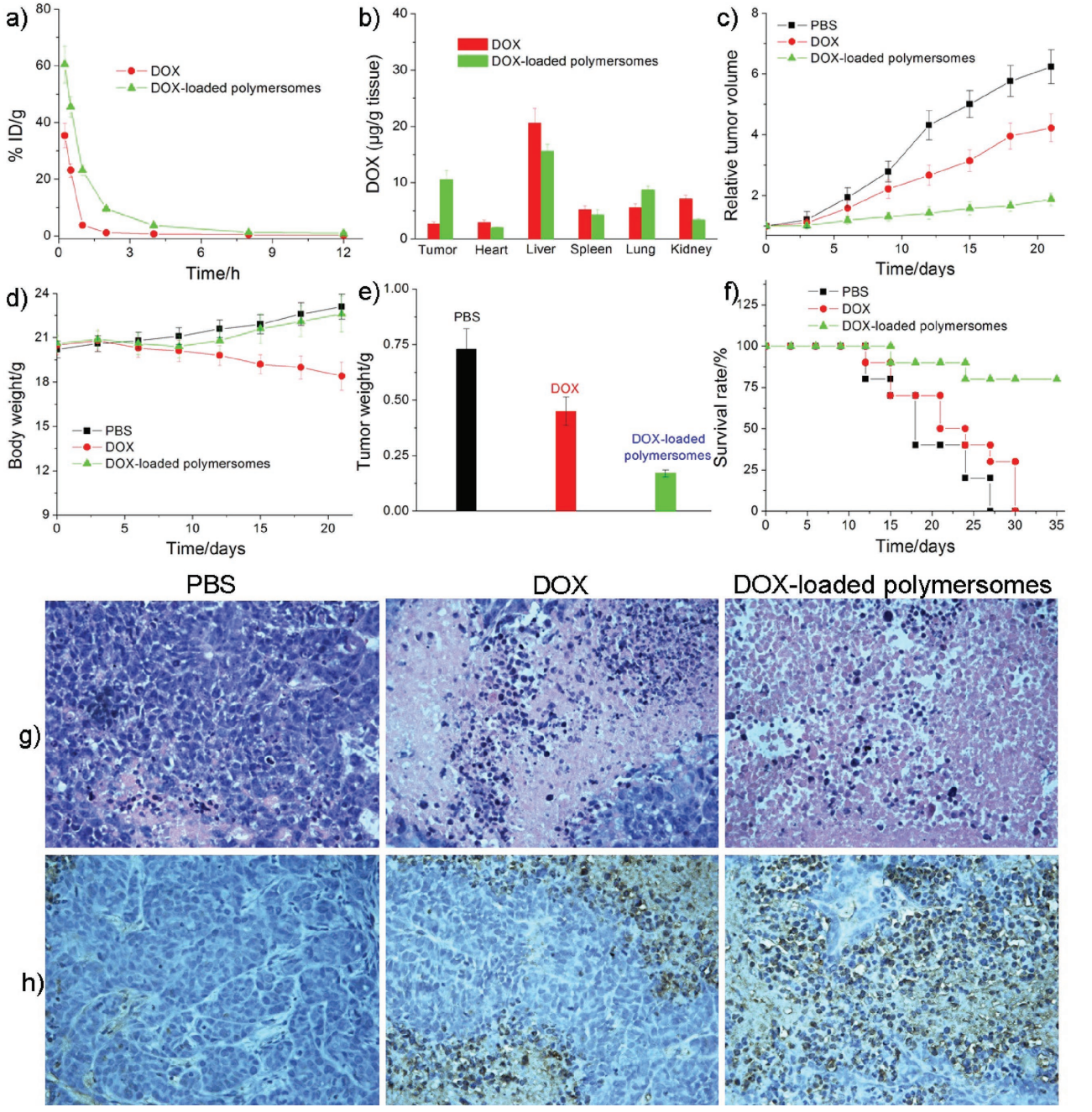

Figure 6. a) Blood circulation time of DOX and DOX-loaded polymersomes analyzed by measuring plasma concentration of DOX after i.v. injection (a dose of 10 mg kg^{-1}). b) Tissue distributions of the DOX in the main organs 12 h after i.v. injection. c) Tumor growth inhibition curves on the HeLa tumor model after various formulations. d) Body weight changes, e) the average weight of the tumors, and f) survival rate of mice bearing HeLa tumors after different treatments. g) H&E and h) TUNEL analyses of tumor tissues after various formulations.

DOX-loaded polymersomes, indicating that DOX-loaded polymersomes could be accumulated in tumor probably due to the EPR effect (Figure 6b). It should be noted that the distribution of DOX in highly perfused organs (lung and liver) was also monitored, arising from the high circulating bloodstream passed through these organs and unavoidable uptake by the reticuloendothelial system (RES).[15]

In order to evaluate that the high tumor accumulation of DOX-loaded polymersomes could enhance its therapeutic efficacy in vivo, we assessed the xenograft tumor growth of HeLa cancer following intravenous administration of free DOX, DOX-loaded polymersomes and phosphate buffer solution (PBS). As shown in Figure 6c, the tumor volumes of the mice administrated with PBS increased rapidly, while DOX and DOX-loaded polymersomes treatment groups inhibited tumor growth to various extents. Compared with that of the PBS group, administration of free DOX resulted in only a slight inhibition of tumor growth (32.2%), while treatment with DOX-loaded polymersomes led to more effective inhibition of tumor growth (70.1%). The final tumor weight was assessed to further validate the effectiveness of DOX-loaded polymersomes formulations (Figure 6e). As expected, the average weight of the tumors was the lowest for the group treated with DOX-loaded polymersomes. The immunohistochemical analyses, including H&E staining and TUNEL assay were employed to assess the antitumor efficacy after treatment with various formulations. The hematoxylin and eosin (H&E) stained sections of tumor tissue from PBS were observed with spindle shape and large nucleus, indicating a rapid tumor growth (Figure 6g). Compared with PBS treated group, both therapeutic groups displayed varying level of necrosis, suggesting that DOX formulations had antitumor effect to some extent (Figure 6g). It was noteworthy that fewer tumor cells and higher level of nuclear shrinkage and fragmentation were observed for the mice treated with DOX-loaded polymersomes. Furthermore, the TUNEL assay showed that DOX-loaded polymersomes treatment induced much more TUNEL-positive cells than the free DOX treated group, which provided convincing evidence for the enhanced efficiency in inducing apoptosis of tumor cells (Figure 6h).

Changes in body weight and survival rate of the tumor-bearing mice after different administrations always reflect the systematic toxicity of different therapy regimens. The high content in normal tissue and low concentration in tumor were responsible to the high systematic toxicity of free DOX. Obviously, the mice treated with free DOX resulted in rapid body weight loss, demonstrating that remarkable side effects were caused (Figure 6d). On the contrary, the mice treated with DOX-loaded polymersomes showed no body weight fluctuation even a slight increase from 20.6 to 22.7 g, indicating that this supramolecular drug delivery system showed negligible systemic toxicity for tumor therapy. In addition, Kaplan-Meier analyses revealed that the median survival of the mice treated with DOX-loaded polymersomes prolonged significantly, which was over 35 days. By contrast, the mice receiving PBS and free DOX had a median survival of 26 and 30 days, respectively (Figure 6f), confirming much less toxicity of DOX encapsulated by the supramolecular polymersomes. In addition, histological analysis of major organ slices (heart, liver, spleen, lung and kidney) of mice treated with PBS, free DOX, and DOX-loaded polymersomes was carried out to further evaluate their systematic toxicity (Figure S31). Compared with the group treated with PBS, no major signs of abnormal damage were observed for the mice treated with DOX-loaded polymersomes, implying low toxicity for the major clearance organs. In contrast, notable cardiotoxicity was observed in terms of free DOX-treated group, which was characterized by cytoplasmic relaxation with small fat drops of cavitation, myocardial swelling, nucleus degeneration and myofibril loose. The in vivo data demonstrated that the antitumor efficacy of DOX was enhanced dramatically and the systematic toxicity toward normal organs was minished effectively upon encapsulation by the polymersomes fabricated from the supramolecular diblock polymer **P5-PEG-Biotin⊃PCL-C_2V**.

3. Conclusion

In summary, we established a novel host–guest recognition motif between a new water-soluble pillar[5]arene (**P5**) and a viologen salt (**C_5V**). The binding affinity between **P5** and **C_5V** decreased significantly by reduction of the dicationic **C_5V** into its cationic radical state due to decreased noncovalent interactions. Based on this novel molecular recognition motif, an amphiphilic supramolecular diblock copolymer (**P5-PEG-Biotin⊃PCL-C_2V**) was fabricated with the PEG segment as the hydrophilic part and the PCL segment as the hydrophobic section. **P5-PEG-Biotin⊃PCL-C_2V** self-assembled to polymersomes in water, which were utilized to encapsulate anticancer drug DOX. The polymersomes exhibited reduction-triggered disassembly, resulting in the release of the anticancer drug. The biotin groups decorating the surfaces of the polymersomes endowed these drug delivery vehicles with excellent targeting ability. In vitro experiments showed that these smart nanocarriers delivered the anticancer drug to biotin receptor-positive cancer cells. After internalization by the cells, the viologen group was reduced into the cationic radical state by NAD(P)H, resulting in the release of the loaded DOX caused by the disassembly of the polymersomes. More importantly, the encapsulation of DOX by polymersomes retained the therapeutic efficacy of DOX towards cancerous cells, while its cytotoxicity towards normal cells was reduced remarkably. In vivo experiments demonstrated that DOX-loaded polymersomes exhibited enhanced accumulation in tumor tissue, dramatically higher antitumor effect and lower systematic toxicity than free DOX in the HeLa tumor xenograft-bearing nude mice. This research provides a novel approach for the construction of stimuli-responsive supramolecular nanocarriers, exhibiting great potential applications in the field of targeted drug delivery.

Supporting Information

Supporting Information is available from the Wiley Online Library or from the author.

Acknowledgements

This work was supported by National Basic Research Program (2013CB834502), the National Natural Science Foundation of China

(21434005 and 91527301), the Fundamental Research Funds for the Central Universities, the Key Science Technology Innovation Team of Zhejiang Province (2013TD02), and Open Project of State Key Laboratory of Supramolecular Structure and Materials (sklssm201611). Animal care and handling procedures were in agreement with the guidelines evaluated and approved by the ethics committee of Zhejiang University. Study protocols involving animals were approved by the Zhejiang University Animal Care and Use Committee.

Received: April 9, 2016
Revised: May 31, 2016
Published online: July 4, 2016

[1] a) M. Ferrari, *Nat. Rev. Cancer* **2005**, *5*, 161; b) V. P. Torchilin, *Nat. Rev. Drug Discovery* **2014**, *13*, 813.

[2] a) P. Horcajada, T. Chalati, C. Serre, B. Gillet, C. Sebrie, T. Baati, J. F. Eubank, D. Heurtaux, P. Clayette, C. Kreuz, J.-S. Chang, Y. K. Hwang, V. Marsaud, P.-N. Bories, L. Cynober, S. Gil, G. Férey, P. Couvreur, R. Gref, *Nat. Mater.* **2010**, *9*, 172; b) H. Yan, C. Teh, S. Sreejith, L. Zhu, A. Kwok, W. Fang, X. Ma, K. T. Nguyen, V. Korzh, Y. Zhao, *Angew. Chem. Int. Ed.* **2012**, *51*, 8373; c) Y. Chen, H. Chen, J. Shi, *Adv. Mater.* **2013**, *25*, 3144; d) C. Alvarez-Lorenzo, A. Concheiro, *Chem. Commun.* **2014**, *50*, 7743.

[3] a) S. Sershen, J. West, *Adv. Drug Delivery Rev.* **2002**, *54*, 1225; b) P. Tanner, P. Baumann, R. Enea, O. Onaca, C. Palivan, W. Meier, *Acc. Chem. Res.* **2011**, *44*, 1039; c) G. Chen, H. Qiu, P. N. Prasad, X. Chen, *Chem. Rev.* **2014**, *114*, 5161; d) X. Ma, Y. Zhao, *Chem. Rev.* **2015**, *115*, 7794.

[4] a) E. Soussan, S. Cassel, M. Blanzat, I. Rico-Lattes, *Angew. Chem. Int. Ed.* **2009**, *48*, 274; b) S. Egli, M. G. Nussbaumer, V. Balasubramanian, M. Chami, N. Bruns, C. Palivan, W. Meier, *J. Am. Chem. Soc.* **2011**, *133*, 4476; c) X. Wang, G. Liu, J. Hu, G. Zhang, S. Liu, *Angew. Chem. Int. Ed.* **2014**, *53*, 3138; d) H. Cabral, K. Miyata, A. Kishimura, *Adv. Drug Delivery Rev.* **2014**, *74*, 35; e) J. Song, P. Huang, H. Duan, X. Chen, *Acc. Chem. Res.* **2015**, *48*, 2506.

[5] a) Q. Yan, R. Zhou, C. K. Fu, H. J. Zhang, Y. W. Yin, J. Y. Yuan, *Angew. Chem. Int. Ed.* **2011**, *50*, 4923; b) Q. Yan, Y. Xin, R. Zhou, Y. Yin, J. Yuan, *Chem. Commun.* **2011**, *47*, 9594; c) X. Ji, S. Dong, P. Wei, D. Xia, F. Huang, *Adv. Mater.* **2013**, *25*, 5725.

[6] a) D.-W. Yoon, D. E. Gross, V. M. Lynch, J. L. Sessler, B. P. Hay, C.-H. Lee, *Angew. Chem. Int. Ed.* **2008**, *47*, 5038; b) Z. Niu, H. W. Gibson, *Chem. Rev.* **2009**, *109*, 6024; c) D. Ma, G. Hettiarachchi, D. Nguyen, B. Zhang, J. B. Wittenberg, P. Y. Zavalij, V. Briken, L. Isaacs, *Nat. Chem.* **2012**, *4*, 503; d) D. Jiao, J. Geng, X. J. Loh, D. Das, T.-C. Lee, O. A. Scherman, *Angew. Chem. Int. Ed.* **2012**, *51*, 9633; e) C. Talotta, C. Gaeta, Z. Qi, C. A. Schalley, P. Neri, *Angew. Chem. Int. Ed.* **2013**, *52*, 7437; f) M. Zhang, X. Yan, F. Huang, Z. Niu, H. W. Gibson, *Acc. Chem. Res.* **2014**, *47*, 1995; g) J. Hu, S. Liu, *Acc. Chem. Res.* **2014**, *47*, 2084; h) S.-K. Ko, S. K. Kim, A. Share, V. M. Lynch, J. Park, W. Namkung, W. V. Rossom, N. Busschaert, P. A. Gale, J. L. Sessler, I. Shin, *Nat. Chem.* **2014**, *6*, 885; i) G. Yu, K. Jie, F. Huang, *Chem. Rev.* **2015**, *115*, 7240; j) R. Dong, Y. Zhou, X. Huang, X. Zhu, Y. Lu, J. Shen, *Adv. Mater.* **2015**, *27*, 498; k) K. Zhu, C. A. O'Keefe, V. N. Vukotic, R. W. Schurko, S. J. Loeb, *Nat. Chem.* **2015**, *7*, 514.

[7] a) D. Cao, Y. Kou, J. Liang, Z. Chen, L. Wang, H. Meier, *Angew. Chem. Int. Ed.* **2009**, *48*, 9721; b) M. Xue, Y. Yang, X. Chi, Z. Zhang, F. Huang, *Acc. Chem. Res.* **2012**, *45*, 1294; c) T. Ogoshi, T.-A. Yamagishi, *Eur. J. Org. Chem.* **2013**, 2961; d) N. L. Strutt, H. Zhang, S. T. Schneebeli, J. F. Stoddart, *Acc. Chem. Res.* **2014**, *47*, 2631; e) Z. Qi, K. Achazi, R. Haag, S. Dong, C. A. Schalley, *Chem. Commun.* **2015**, *51*, 10326.

[8] a) C. Li, L. Zhao, J. Li, X. Ding, S. Chen, Q. Zhang, Y. Yu, X. Jia, *Chem. Commun.* **2010**, *46*, 9016; b) Z. Zhang, Y. Luo, J. Chen, S. Dong, Y. Yu, Z. Ma, F. Huang, *Angew. Chem. Int. Ed.* **2011**, *50*, 1397; c) H. Li, D.-X. Chen, Y.-L. Sun, Y. Zheng, L.-L. Tan, P. S. Weiss, Y.-W. Yang, *J. Am. Chem. Soc.* **2013**, *135*, 1570; d) G. Yu, Y. Ma, C. Han, Y. Yao, G. Tang, Z. Mao, C. Gao, F. Huang, *J. Am. Chem. Soc.* **2013**, *135*, 10310; e) W. Si, Z.-T. Li, J.-L. Hou, *Angew. Chem. Int. Ed.* **2014**, *53*, 4578.

[9] a) G. Yu, X. Zhou, Z. Zhang, C. Han, Z. Mao, C. Gao, F. Huang, *J. Am. Chem. Soc.* **2012**, *134*, 19489; b) Q. Duan, Y. Cao, Y. Li, X. Hu, T. Xiao, C. Lin, Y. Pan, L. Wang, *J. Am. Chem. Soc.* **2013**, *135*, 10542; c) H. Zhang, X. Ma, K. T. Nguyen, Y. Zhao, *ACS Nano* **2013**, *7*, 7853.

[10] a) H. Zhang, Y. Zhao, *Chem. Eur. J.* **2013**, *19*, 16862; b) G. Yu, K. Jie, F. Huang, *Chem. Rev.* **2015**, *115*, 7240; c) X. Chi, G. Yu, X. Ji, Y. Li, G. Tang, F. Huang, *ACS Macro Lett.* **2015**, *4*, 996.

[11] R. J. Dinis-Oliveira, C. Sousa, F. Remião, J. A. Duarte, A. S. Navarro, M. L. Bastos, F. Carvalho, *Free Radical Biol. Med.* **2007**, *42*, 1017.

[12] a) N. Sim, D. Parker, *Chem. Soc. Rev.* **2015**, *44*, 2122; b) Y.-X. Wang, D.-S. Guo, Y.-C. Duan, Y.-J. Wang, Y. Liu, *Sci. Rep.* **2015**, *5*, 9019; c) Y.-X. Wang, Y.-M. Zhang, Y.-L. Wang, Y. Liu, *Chem. Mater.* **2015**, *27*, 2848; d) R. Kumar, W. S. Shin, K. Sunwoo, W. Y. Kim, S. Koo, S. Bhuniya, J. S. Kim, *Chem. Soc. Rev.* **2015**, *44*, 6670.

[13] a) P. Huang, D. Wang, Y. Su, W. Huang, Y. Zhou, D. Cui, X. Zhu, D. Yan, *J. Am. Chem. Soc.* **2014**, *136*, 11748; b) J. Song, P. Huang, H. Duan, X. Chen, *Acc. Chem. Res.* **2015**, *48*, 2506; c) J. Song, X. Yang, O. Jacobson, P. Huang, X. Sun, L. Lin, X. Yan, G. Niu, Q. Ma, X. Chen, *Adv. Mater.* **2015**, *27*, 4910.

[14] a) P. Huang, J. Lin, X. Wang, Z. Wang, C. Zhang, M. He, K. Wang, F. Chen, Z. Li, G. Shen, D. Cui, X. Chen, *Adv. Mater.* **2012**, *24*, 5104; b) P. Huang, J. Lin, W. Li, P. Rong, Z. Wang, S. Wang, X. Wang, X. Sun, M. Aronova, G. Niu, R. D. Leapman, Z. Nie, X. Chen, *Angew. Chem. Int. Ed.* **2013**, *52*, 13958; c) X. Hu, J. Hu, J. Tian, Z. Ge, G. Zhang, K. Luo, S. Liu, *J. Am. Chem. Soc.* **2013**, *135*, 17617; d) G. Yu, W. Yu, Z. Mao, C. Gao, F. Huang, *Small* **2015**, *11*, 919.

[15] a) H. J. Kim, H. Takemoto, Y. Yi, M. Zheng, Y. Maeda, H. Chaya, K. Hayashi, P. Mi, F. Pittella, R. J. Christie, K. Toh, Y. Matsumoto, N. Nishiyama, K. Miyata, K. Kataoka, *ACS Nano* **2014**, *8*, 8979; b) Y. Tian, X. Jiang, X. Chen, Z. Shao, W. Yang, *Adv. Mater.* **2014**, *26*, 7393; c) P. Huang, W. Wang, J. Zhou, F. Zhao, Y. Zhang, J. Liu, J. Liu, A. Dong, D. Kong, J. Zhang, *ACS Appl. Mater. Interfaces* **2015**, *7*, 6340.